The Bioscan AN INTERNATIONAL QUARTERLY JOURNAL OF LIFE SCIENCES 21(1) 1087-1125, 2026 www.thebioscan.com

Physicochemical and multitechnique characterisation of Structural, functional, optical, Thermal, Microbiological, Elemental, mechanical and Antibacterial properties of L-Asparagine monohydrate admixtured with Oxalic acid dihydrate with a focus on nonlinear optical applications

N. Rajasekar [1], K. Balasubramanian [2*]

[1]Research scholar (Reg.No: 22211072131006), PG and Research department of physics, The M.D.T Hindu college, Pettai, Tirunelveli-627010, Tamilnadu, India. E-mail : rs9012618@gmail.com

[2]The Principal and the Head, PG and Research department of physics, The M.D.T Hindu college, Pettai, Tirunelveli-627010, Tamilnadu, India.*

[1,2]Affiliated by ManonmaniamSundarnar University, Abishekapatti-627012, Tirunelveli, Tamilnadu, India.*

***Corresponding author** : K. Balasubramanian

Graphical abstract

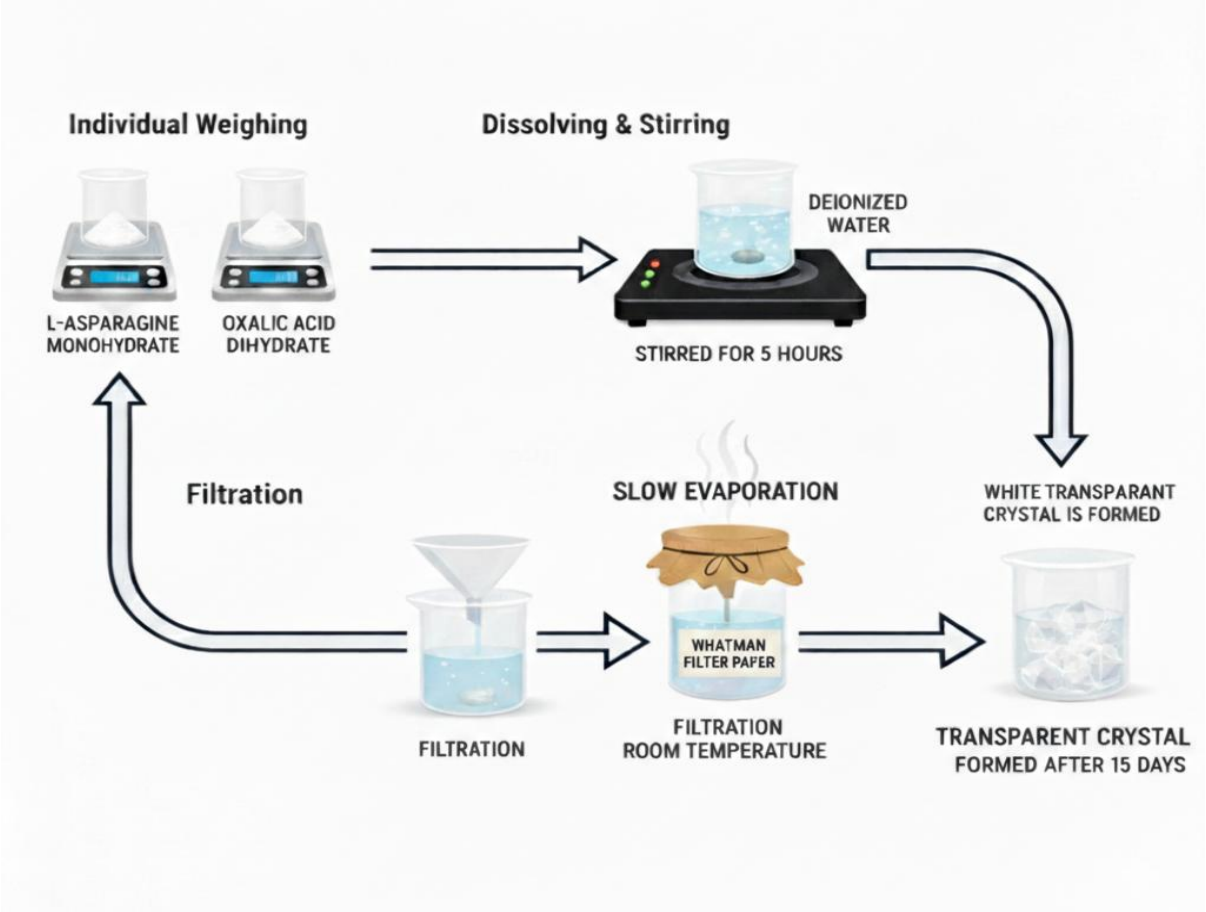

https://doi.org/10.63001/tbs.2026.v21.i01.pp1087-1125

KEYWORDS

W-H method, functional, optical, Thermal kinetic parameters : Kissinger method, mechanical, Biological properties, Photonics, opto electronics and Nonlinear optical applications.

Received on: 13-12-2025

Acceptedon:06-02-2026

Published on: 14-02-2026

ABSTRACT

L-Asparagine monohydrate admixtured with oxalic acid dihydrate (LASPOD) crystals were successfully grown and comprehensively analyzed to investigate their structural, optical, and thermal properties. Single crystals were obtained by the slow evaporation method under ambient conditions, yielding transparent and well shaped crystals. The crystallographic structure and unit cell parameters were derived from powder XRD. Powder XRD was employed to estimate the crystallite size and microstrain of L-Asparagine oxalic acid dihydrate, using the williamson-Hall (W-H) plot method to separate the contribution of crystallite size and strain. The various assignement peak, functional and amino acids groups are identify by using the FTIR. In, UV-DRS studies the various graphs are plotted such as Absorbance, Transmittance (%), Refractive index, and Reflectance. SEM revealed the morphological features of the crystal surface. The TG-DTA curves revealed multi step decomposition, indicating good thermal stability upto a certain temperature. Decomposition Kinetic parameters, such as the activation energy (E_a) and the Arrhenius pre-exponential factor (A), were evaluated using the Broido method, providing insight to the decomposition mechanism. The Carbon, Nitrogen and oxygen elemental composition was confirmed by EDAX analysis. Photoluminescence analysis shows a highest emission peak at 466 nm, confirming excellent optical quality with reduced defect density in the as-grown crystals. Z-scan analysis reveals a clear nonlinear optical response of the crystal under laser excitation. The molecular configuration of LASPOD was validated through ^{1}H and ^{13}C FT NMR spectroscopy. The antibacterial potential was evaluated against selected bacterial strains to determine the material's bioactive efficiency.

Introduction

L-Asparagine oxalate dihydrate ($LAO.2H_2O$) is an organic NLO crystal obtained through the interaction between the amino acid L- Asparagine with Oxalic acid **[1, 2]**. The presence of hydrogen bonding, polar functional groups ($-NH_2$, -COOH), and crystalline asymmetry in $LAO.2H_2O$ contributes to its non-centrosymmetric crystallographic arrangement, which is crucial for Third harmonic generation (THG). L-Asparagine is an simplest amino acid that primirly exhibits THG rather than SHG efficiency **[3]**. Organic acid such as oxalic acid dehydrate and amino-acid based NLO crystal are of interest owing to their strong nonlinear optical response, and fast response behavior **[4]**. L-Asparagine oxalate Dihydrate ($LAO.2H_2O$) has been extensively investigated by various characterization methods, such as Powder-XRD, Fourier transform infrared spectroscopy, Ultraviolent- DRS, Scanning electron microscopy, EDX, Thermogravimetric-Differential thermal analysis, Z-scan, 1H and 13C FT-NMR, CHN, Microhardness measurements, and Photoluminescence to explore its structural,

optical and mechanical properties **[5]**. LASPOD is widely used for NLO applications including optical limiting, Laser devices, and Photonics applications, due to its favorable crystal structure, optical transparency and thermal stability **[6]**. The thermal behaviour and kinetic parameters of L-Asparagine oxalate dehydrate were analyzed using TG-DTA, and the activation energy (E_a), the enthalpy (ΔH), the entropy (ΔS) and Gibbs free energy (ΔG) were its thermal stability and decomposition mechanism **[7]**. These thermal parameters provide insight into the decomposition mechanism and structural stability of the crystal under heat, which is crucial for its performance in NLO applications. Stable thermal behaviour ensures that the crystal can tolerate high-intensity laser exposure, making it suitable for optical limiting, photonic devices applications **[8]**.

Crystal synthesis

L-Asparagine oxalate dihydrate crystals were prepared by dissolving L-Asparagine and oxalic acid dihydrate in a (1:1) equimolar ratio. The equimolar amounts of L-Asparagine and oxalic acid was dissolved in an appropriate amount of deionized water as the solvent to ensure homogeneity. The prepared homogeneous solution was stirred continuously for a duration of 6 h to achieve complete dissolution and homogeneous mixing. Finally, the solution was filtered using whatmann filter paper to eliminate insoluble impurities, and the clear filtrate was retained for crystallization. The resultant mixture was allowed to evaporate naturally under ambient temperature, facilitating crystal formation. L-Asparagine oxalate dihydrate exhibited rapid nucleation, with crystal growth initiated within 12-15 days, even from a very small amount of solvent.

The molecular formula for L- Asparagine oxalate dihydrate

L-Asparagine monohydrate – $C_4H_8N_2O_3.H_2O$

Oxalic acid dihydrate – $C_2H_2O_4.2H_2O$

L- Asparagine oxalate dihydrate is $C_6H_{16}N_2O_{10}$

Fig 1. Photographic image of L-Asparagine oxalate dihydrate single crystals

Results and discussion

1). Powder XRD

In P-XRD is a widely used analytical technique employed for investigating crystallographic structure in crystalline material. By this method, a powdered sample is exposed to X-rays, and the diffraction pattern produced is recorded. From this pattern, the crystal structure and Phase identification can be elucidated, along with the Unit cell parameters, Degree of crystallinity, Crystallite size and Lattice microstrain, by employing the Willaimson-Hall method. The observed diffraction peaks corresponding to L-Asparagine monohydrate were indexed and found to be in excellent aggrement with the standard JCPDS card No.(30-1529). The obtained peaks of oxalic acid dihydrate were consistent with the standard JCPDS card No. (04-0621). The prominent diffraction peaks observed in the PXRD pattern were indexed to the different (hkl) peaks are (13.625), (19.906), (22.547), (26.598), (27.394), (30.444), (37.932), (40.777), (43.623), (54.160) and (55.572).The highest intensity diffraction peak was observed at a 2θ value of (22.547), corresponding to the (2 2 0) plane **[9, 10]**.

The lattice parameters such as the unit cell dimensions a= 6.34 A° , b = 7.27 A° ,c = 10.56 A° , and interaxial angles α = 93.89 ° ,β = 100.19 ° ,ϒ = 98.14 ° ,along with the number of formula units per unit cell (z) and the unit cell volume (V) = 472 A°, the corresponding parameters were determined from powder X-ray diffraction (PXRD) data, using the least-squares refinement, and the refined values show consistent with previously reported in the literature **[11]**.

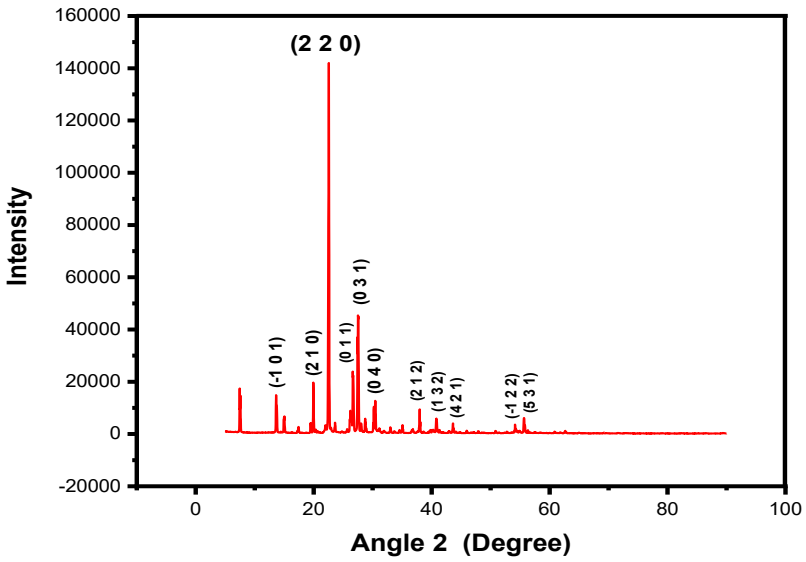

Fig. 2(a) PXRD spectrum of the grown crystal

The Williamson-Hall method was utilized to estimate the crystallite size and lattice strain based on the widening of PXRD peaks.

Willaimson-Hall formula is

$$\beta.\cos\theta = K\lambda/D + 4\epsilon.\sin\theta \quad (1)$$

Where the formula explanations are β is FWHM of the peak, θ be a Bragg angle, K is shape factor, λ is X-ray wavelength, d is crystalline size and ϵ be the Lattice strain.

$$\delta = 1/D^2 \quad (2)$$

The crystallite size of LASPOD was calculated through Debye–Scherrer's formula;

Here, the constant, k = 0.9, λ = 1.5405 Å & β represents the full width at half maximum (FWHM). The X-ray diffraction (XRD) pattern indicates that the most intense peak occurs at 2θ = 19.79°.

$$D = k\lambda / \beta\cos.\theta \quad (3)$$

The value of Slope is lattice strain

In the Williamson-Hall plot, β.cosθ was plotted on the Y-axis against 4ϵ.sinθ along the X-axis, where the slope gives the lattice strain and the intercept provides the crystallite size using D = Kλ / intercept

The willaimson-Hall (W-H) analysis was performed to assess crystallographic properties of the sample. The results demonstrate that the material possesses a well-defined crystalline structure with minimal microstrain and a moderate dislocation density. The analysis further reveals a high degree of crystallinity, suggesting a well-ordered atomic arrangement within the crystal lattice. These features collectively confirm the excellent structural quality and thermal stability of the synthesized material, making it suitable for potential applications requiring superior crystallinity and structural integrity **[12]**. Fig 2 (a) and fig 2 (b) show the powder XRD pattern and the williamson-Hall (W-H) plot of the material, respectively. Table 2. Lists the parameters derived from Williamson Hall (W-H) plot analysis of the sample.

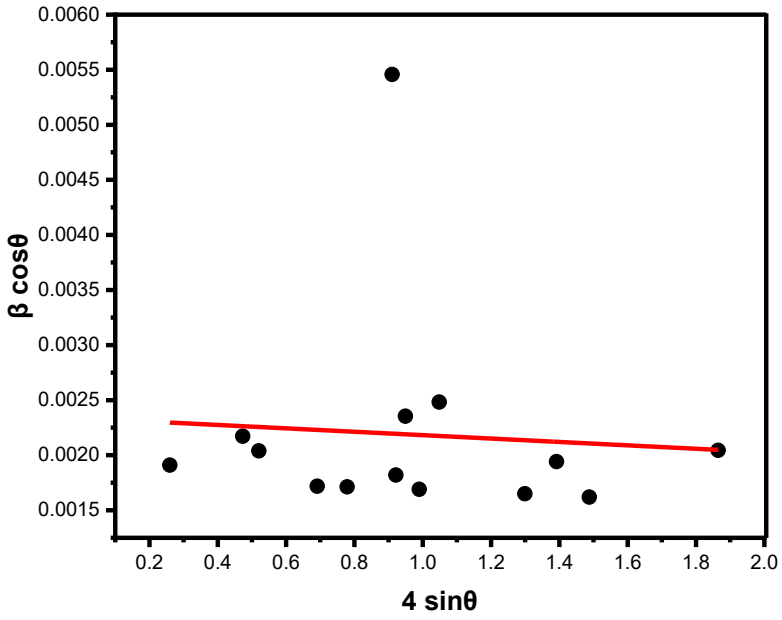

Fig 2 (b) Hall willaimson plot of the synthesized crystal

Table : 2

Listed the Williamson-Hall plot values of the material

Structural parameters	**values**
Maximum peak (2θ)	22.547
FWHM (β)	0.00234 radians
Crystallite size	59.3 nm
Dislocation density (δ)	2.85 x 10^{10} cm^{-2}
Microstrain (η)	1.54393 x 10^{-4}
Degree of crystallinity	89.7 %

2). Fourier transform infrared studies

The FTIR spectroscopy of single crystalline L-Asparagine monohydrate admixtured with oxalic acid dihydrate was acquired over the wavenumber range of 400-3500 cm^{-1} to characterization of characteristic molecular vibrations present within the crystal lattice. A absorption band near 478.11 cm^{-1} is assigned to skeletal vibrations involving C-C-C bending through out the crystal lattice **[13]**. The featured at 597.12 cm^{-1} corresponds to C-C-C bending and C-N-C bending vibrations of the amino acid backbone. The spectral feature at 624.28 cm^{-1} is attributed C-N stretching and N-H wagging modes. The spectral band at 651.50 cm^{-1} is assigned to out-of-plane CH_2 bending vibrations. The feature at 706.90 cm^{-1} is indicative of CH_2 rocking and COO- bending vibrations. The peal at 834.13 cm^{-1} is assigned to CH_2 wagging and C-H bending motions. The absorption at 880.30 cm-1 arises from N-H wagging and C-H bending vibrations. A band centred at 1053.69 cm^{-1} is assigned to C-O stretching and C-N stretching vibrations of the amino acid **[14]**. The absorption at 1208.61 cm^{-1} is associated with C-N and C- stretching vibrations. A spectral peak around 1363.54 cm^{-1} is attributed to symmetric stretching of the carboxylate (COO-) groups. The peak observed at 1409.71 cm^{-1} arises from CH_2 bending and asymmetric stretching of COO- groups. The spectral region at 1527.70 cm^{-1} is assigned to N-H bending vibrations of amino groups (amide II band). The absorption at 1591.31 cm^{-1} represents asymmetric stretching of COO- groups **[15]**. An absorption around 1674.41 cm^{-1} corresponds to C=O stretching of the amide functional group (amide I band). The absorption region around 1728.79 cm^{-1} is assigned to C=O stretching vibration of the carboxylic acid group of oxalic acid. An absorption around 1892.95 cm^{-1} is associated with O-H bending and lattice water vibrations. A spectral band around 2841.99 cm^{-1} corresponds to symmetric C-H stretching of CH_2 groups. An absorption around 2979.48 cm^{-1} is attributed to asymmetric C-H stretching of CH_2 and CH_3 groups. An absorption features at 3188.78 cm^{-1} corresponds to N-H stretching vibrations of amino groups involved in hydrogen bonding. The broad absorption at 3399.11 cm^{-1} represents O-H stretching vibrations of water molecules within the crystal lattice **[16]**. Fig. 3 depicts the FTIR spectrum for the investigated material, illustrating the characteristic molecular vibrations of the compound.

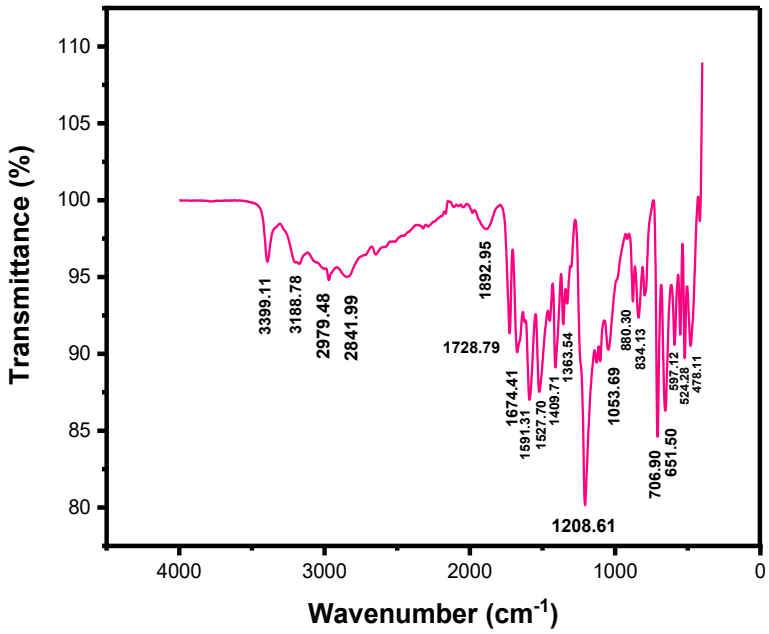

Fig 3. FTIR graph of the sample showing characteristic functional groups

3). UV-DRS

The optical response of the synthesized material was systematically investigated by Ultraviolet-diffuse reflectance spectroscopy (UV-DRS) in the spectral range of 200 - 800 nm **[17]**. The recorded wavelength profile reveals a well-defined absorption edge with a cut-off wavelength at 256 nm, indicating pronounced absorption within the ultraviolet spectral region along with High optical transparency in the visible and near-infrared regions, such a sharp absorption edge is an essential requirement for optical and optoelectronic materials, as it reflects minimal defect-induced absorption and good crystalline quality. The observed spectrum in the Ultraviolet spectral region is ascribed to electronic transitions to the molecular framework of the crystal, predominantly the (n-$\sigma*$) and (n-π^*) transitions arising from the presence of alcohol (-OH) functional moieties along with other nonbonding electrons associated with heteroatoms.

Furthermore, the wavelength versus transmittance behaviour derived from the reflectance data demonstrates a maximum transmittance approaching 100% across the complete visible spectral range, confirming the excellent optical transparency exhibited by this material **[18]**. High optical transmission across the visible and near-infrared spectral region suggests low optical scattering and minimal absorption losses, which are crucial for device fabrication. The absence of significant absorption bands beyond the cutoff wavelength further suggests that the crystal is

free devoid of color centers as well as impurity-related defects. Overall, the superior optical transparency, wide transmission window, and well-defined UV cutoff wavelength highlight the potential applicability of the crystal in utilization in optoelectronic, photonic, along with nonlinear optical applications, including frequency conversion and optical switching applications **[19]**.

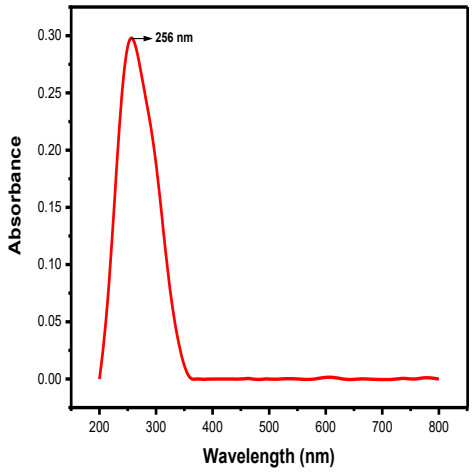

Figure. 3 (a) Wavelength vs Absorbance

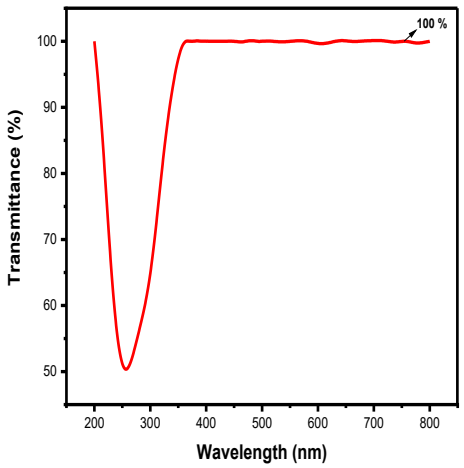

Figure. 3 (b) Wavelength vs Transmittance (%)

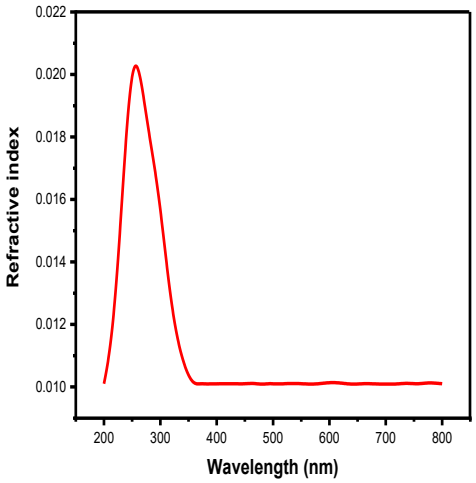

Fig. 3 (c) Wavelength vs Refractive index

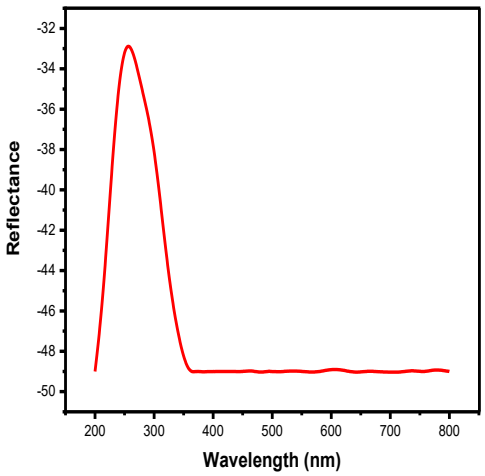

Fig. 3 (d) Wavelength vs Reflectance

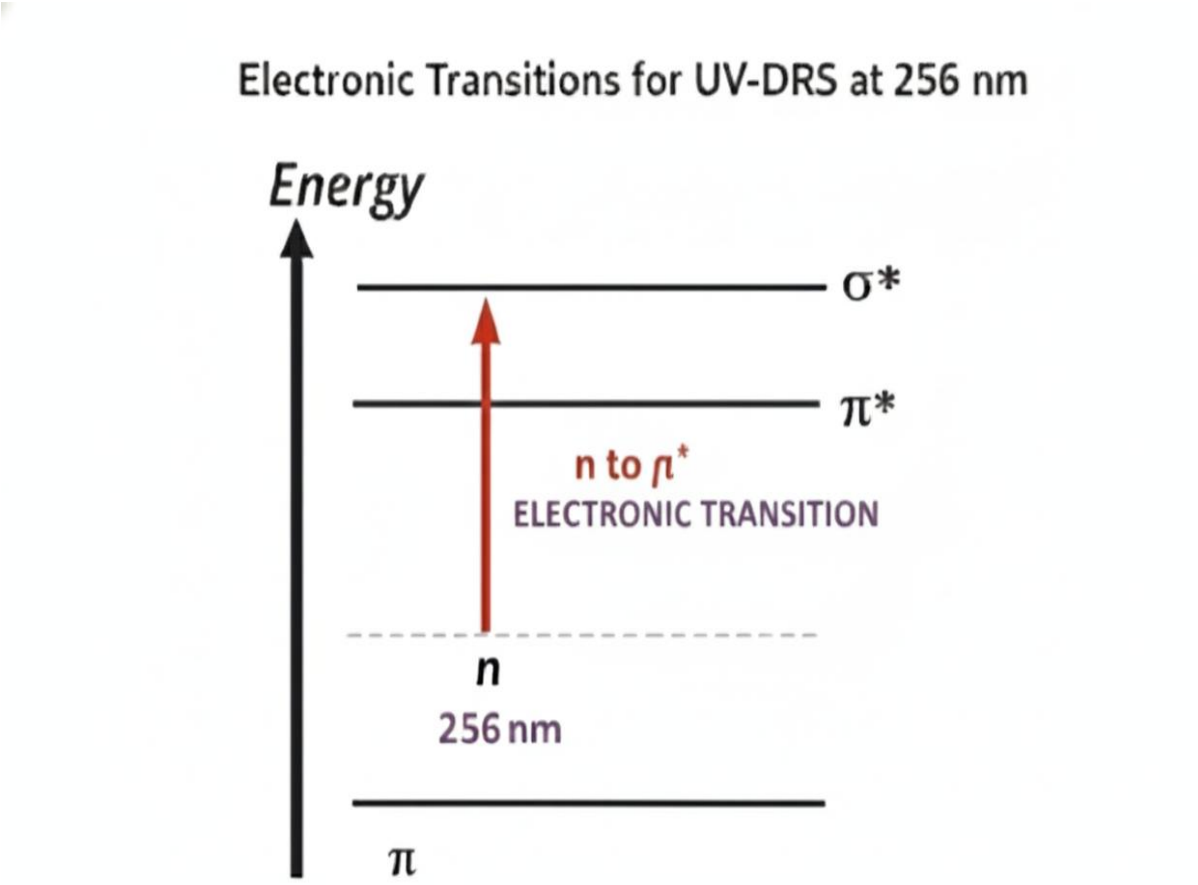

Fig. 3 (d) Schematic representation of electronic excitations in the material

The optical response of the prepared material was comprehensively investiagted to understand their light propagation characteristics. The wavelength-dependent variation in refractive properties reflects the dispersive nature of the crystals, indicating subtle changes in polarizability across the examined spectral range. Such behaviour is important for evaluating the transparency and optical uniformity of the crystals, which are critical parameters for potential applications in photonics and optoelectronic devices **[20]**.

UV-DRS was employed to study the wavelength –dependent reflectance exhibited by the crystals. The observed trends reveal how the crystal surface interacts with incident light and provide insight into absorption characteristics within the material. These observations remain essential in elucidating the overall optoelectronic performance of the crystals and their suitability for applications where efficient light management and surface optical properties are required **[21]**.

4). SEM

The surface microstructure of the grown L-Asparagine oxalate dihydrate was characterized using scanning electron microscopic technique **[22]**. The micrographs exhibited a well-developed surface with clearly visible crystalline feature, indicating

the good growth of the sample. The presence of smooth facts and regular morphology further corroborates the crystalline phase of the sample. Such surface characteristics exerts a significant influence on the optoelectronic and mechanical characteristics of the crystal, making SEM analysis an essential tool for evaluating its suitability for opto-electronic applications **[23]**. Fig 5 (a) to Fig 5 (e) show the SEM images corresponding to the samples, illustrating the surface morphology and microstructural features.

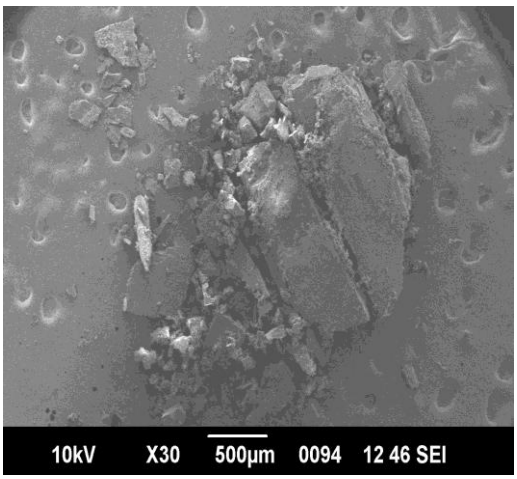

Fig 5 (a) SEM micrograph

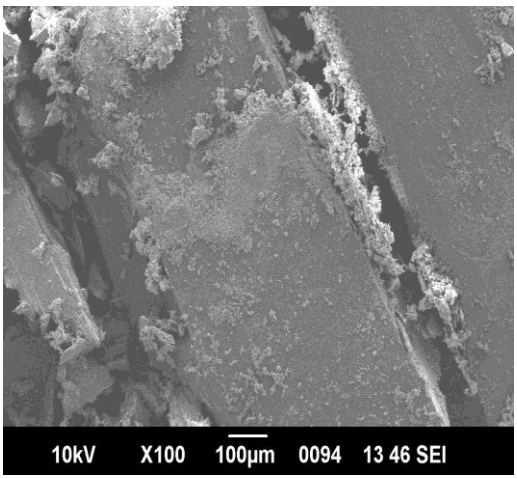

Fig 5 (b) SEM micrograph

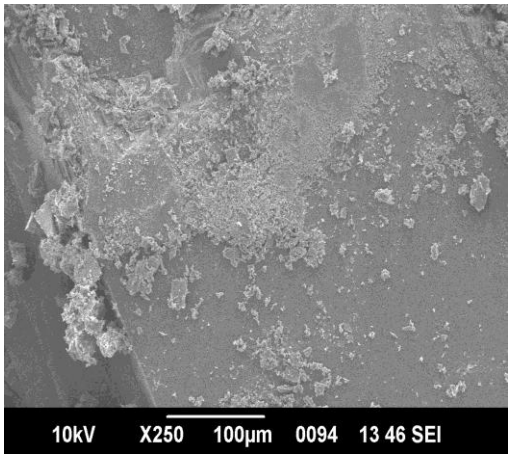

Fig 5 (c) SEM micrograph

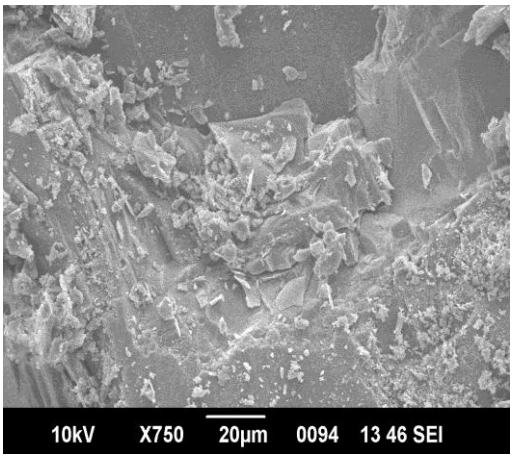

Fig 5 (d) SEM micrograph

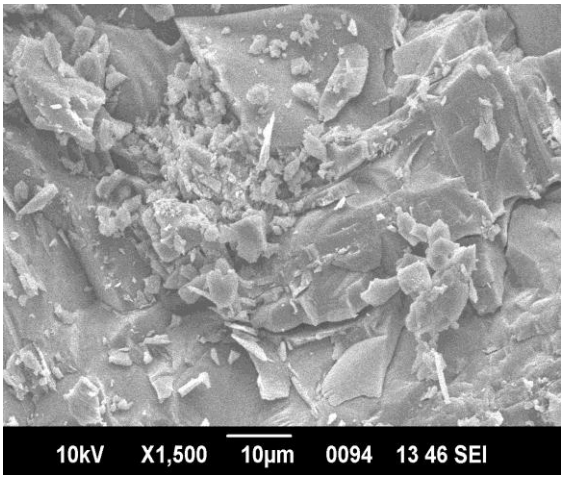

Fig 5 (e) SEM micrograph

5). EDX analysis

EDX analysis is an analytical tool used along with SEM for atomic compositional analysis of the material **[24]**. When the crystal is bombarded with an electron beam, each element presents emits characteristics X-rays. By detecting these X-rays, EDX provides both quantitative (which elements are present) and Quantitative (their relative proportions) information. EDX studies was performed to examine the atomic constituent within the material, confirming the presence of carbon, nitrogen and oxygen other constitute without any detectable impurities.

EDX spectroscopy was utilized to determine atomic constituents of the prepared sample. The results confirmed the observation of carbon, nitrogen, and oxygen as the principal elements, with their respective contributions aligning closely with the expected stoichiometric ratios. The total weight and atomic percentages of these elements accounted for 100 %, indicating the high chemical purity of the material and the successful incorporation of the desired elements within the crystal lattice **[25]**. Fig. 6 shows the EDAX spectrum of the material displaying the composition along with the corresponding weight and atomic percentages. Table. 4 presents the elemental constituents within the material from EDAX technique.

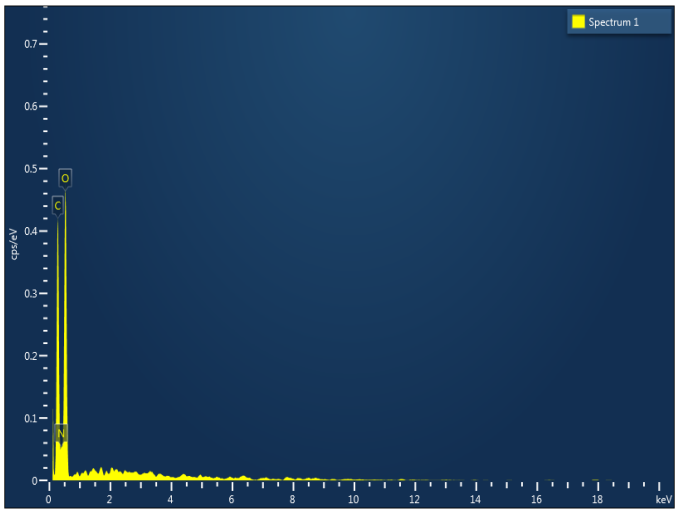

Fig 6. EDAX spectrum showing atomic constituents of the crystal

Table : 4

Elemental constituent of the material determined by EDAX technique

Element	Line Type	Wt %	Atomic %
C	K series	39.97	46.72
N	K series	4.94	4.95
O	K series	55.09	48.34
Total:		**100**	**100**

6). TG-DTA

The term TG-DTA studies are important thermal techniques employed to evaluate the heat stability and decomposition behaviour of crystals **[26]**.

Thermogravimetric (TG) monitors variations in mass of the sample with increasing temperature, thereby providing information on moisture content, heat stability along with successive decomposition processes.

Differential thermal analysis (DTA) is a thermal method used to study phase transitions, melting, crystallization, and decomposition of materials by recording endothermic and exothermic events during heating. It offers valuable information

regarding heat stability and structural changes of the prepared sample, which are crucial for their optical and electronic applications **[27]**.

TG-DTA were performed on the crystal, with an precisely measured mass of 4.553 mg, to investigate its thermal stability and decomposition behavior. During DTA measurement, a thermal event was recorded at 20 - 800℃ representing structural changes in the material. In DTA graph the prominent endothermic peak observed around 428℃ arises from the endothermic transition inherent to the crystal structure, the DTA profile exhibits a distinct thermal event at 480℃, indicating a phase transformation, A third peak appeared at 558℃ in the DTA analysis, confirming the decomposition stage. The DTA thermogravimetric exhibited a peal at 621℃, indicative of the melting/ decomposition process **[28]**. Fig 7 (a) presents the TG-DTA curve with weight (%) plotted against Heat flow endo downward.

TG curve shows a first stage weight loss at 162 ℃, indicative of the dehydration of the material, The second stage of mass loss occurs around 249 ℃ which is corresponds to the initial decomposition of the organic component or partial breakdown of the molecular framework. The third stage stage of the mass loss recorded at 379 ℃ corresponds to the further decomposition of the organic structure, and final stage of mass loss appearing around 576 ℃ represents the complete degradation of the material, possibly leading to the formation of a stable residue such as carbonaceous or inorganic remnants.

The DTG analysis of L-Asparagine oxalate dihydrate crystals showed multiple thermal events. The first weight-loss peak at 209.23℃ indicated initial decomposition, likely arising from the loss of water molecules. The second transition occurs at 350.11℃ corresponded to furher breakdown of the organic framework. An exothermic peak at 419.05℃ suggested energy release associated with structural reorganization, while the final peak at 519.30℃ represented the entire thermal breakdown of the sample. These observations provide insight into the heat stability and degradation behavior of the sample**.** Fig 7 (b) shows the Derivative thermogravimetric (DTG) curve showing temperature celsius versus derivative weight (%). Fig 7(c). depicts thermal analysis using the Kissinger method.

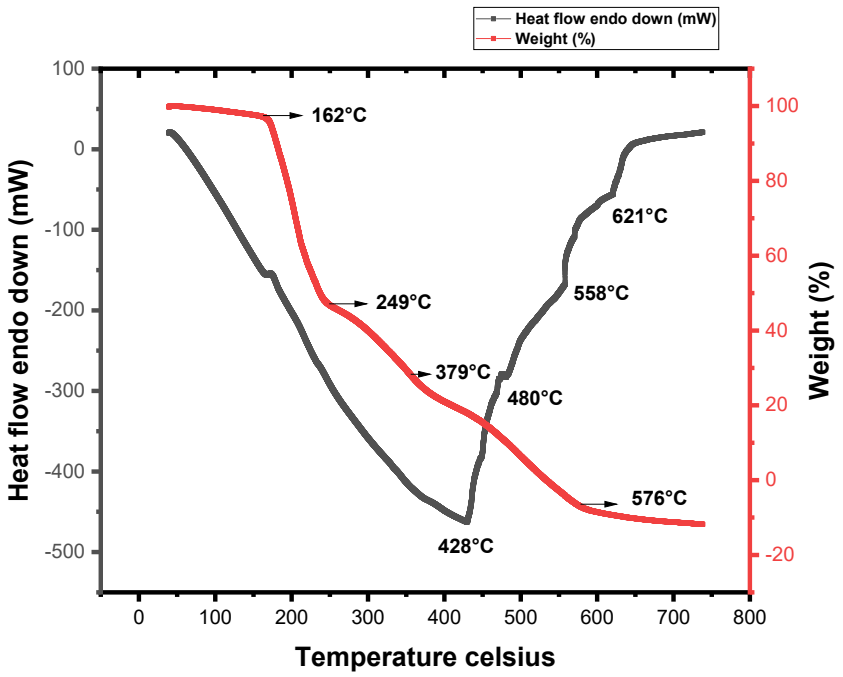

Fig 7 (a). TG-DTA curve - weight (%) versus Heat flow endo downward

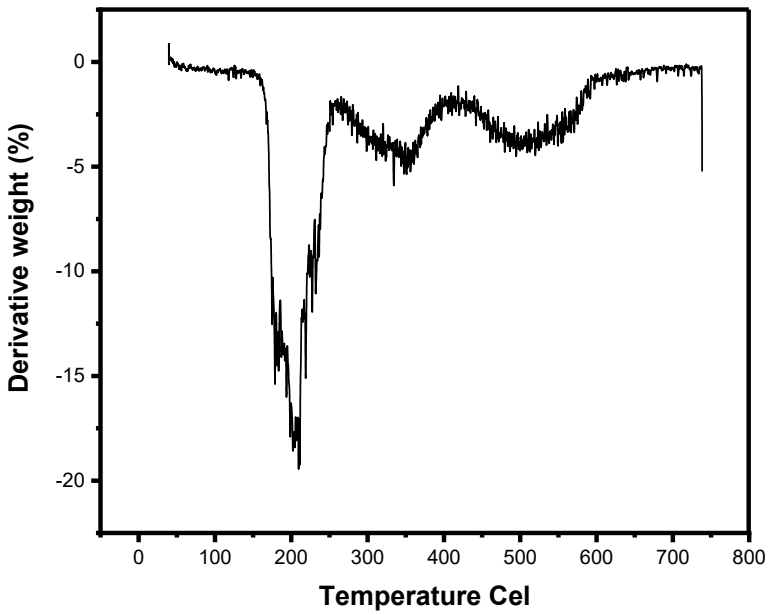

Fig 7 (b). Derivative thermogravimetric (DTG) curve showing temperature celsius versus derivative weight (%)

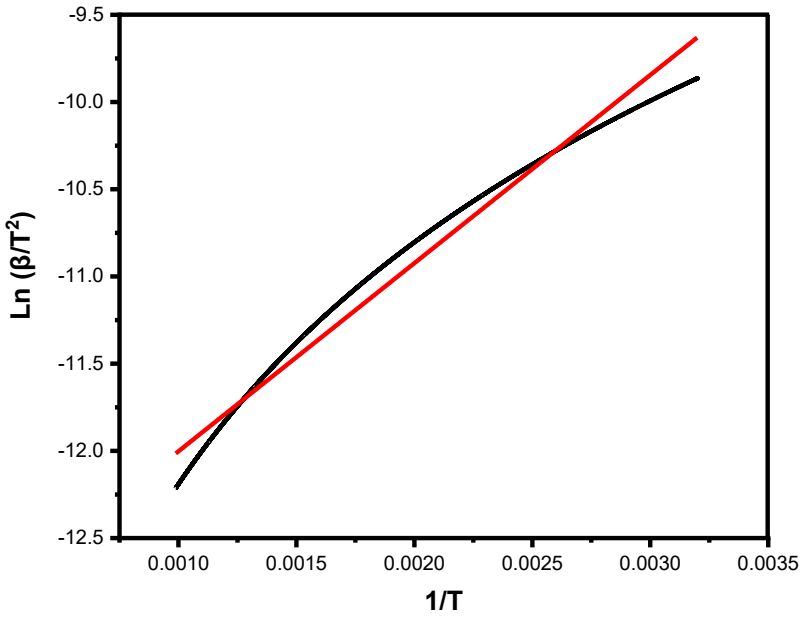

Fig 7 (c). Thermal analysis using the Kissinger method

Table 6

Kinetic thermal parameters of kissinger method

Kinetic parameters	**Values**
Slope	1078.61705
Temperature in Kelvin	505.86
Frequency factor in (A) sec^{-1}	2.25 x 10^{-3}
Activation energy (Ea) in J/mol^{-1}	8962.5
Entropy of activation (ΔS) in J/mol^{-1}	-300
Enthalpy of activation (ΔH) in J/mol^{-1}	4762
Gibbs free energy (ΔG) in J/mol^{-1}	156349

The Kissinger method was employed to analyze the TG-DTA of the sample in order to

investigate its thermal decomposition kinetics **[29]**. This approach enabled determination of key kinetic parameters, including energy of activation (Ea), enthalpy (ΔH), entropy (ΔS), and gibbs free energy (ΔG), thereby providing an detailed insight into the energetic and mechanistic aspects of the decomposition process. The analysis highlights the stepwise nature of the thermal events and offers valuable understanding of the thermal stability and reactivity exhibited by the material at elevated temperatures **[30].**

7). CHN analysis

CHN analysis is very important because it helps confirm the elemental composition and purity of the prepared sample, especially when the crystals are organic **[31]**. A 7.28 mg portion of the LASPOD crystal was subjected to CHN elemental analysis to evaluate its elemental composition. CHN analysis gives experimental % of Carbon, Nitrogen and Hydrogen. The experimental CHN analysis of the prepared sample was consistent with theortical values, validating the expected composition of carbon, hydrogen and nitrogen. This analysis acts as a purity check for your grown crystal **[32]**. L-Asparagine oxalate dihydrate consists of the elements carbon, Nitrogen and oxygen with the molecular formula $C_6H_{14}N_2O_9$. Fig. 8 shows the molecular structure of L-asparagine oxalate dihydrate. Table. 7 presents the CHN analysis of the synthesized sample, showing carbon, nitrogen and hydrogen elements percentages.

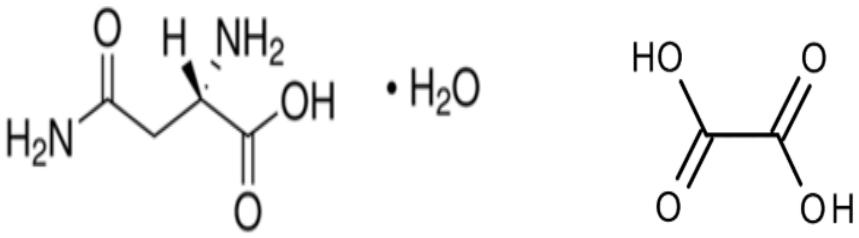

Fig. 8 molecular structure of L-asparagine oxalate dihydrate

Table : 7

Elemental (CHN) analysis of the synthesized sample showing carbon, hydrogen and nitrogen content

Sample weight (mg)	Carbon %	Hydrogen %	Nitrogen %
7.28 mg	**31.78 %**	**5.64 %**	**12.01**

8). Z scan technique in liquid

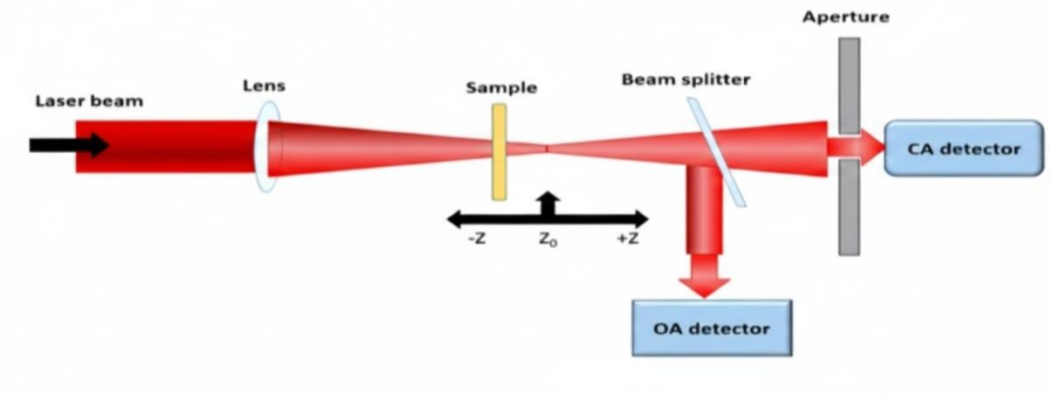

Fig. 9 (a) Z-Scan experimental setup diagram

The Z-scan studies is a widely adopted experimental approach for evaluating the third-order nonlinear optical (NLO) charactersitics exhibited by the sample, including both nonlinear absorption coefficient and Nonlinear refractive index **[33]**. The Z scan technique entails moving a sample along the foca (Z-axis) of a laser radiation and recording the transmitted intensity through a finite aperture closed or open aperture **[34]**. The intensity-dependent variations in transmittance results from the nonlinear interation exhibited by the sample with the incoming laser beam. The Z-scan mainly used in optical limiting materials, photonics and optoelectronic devices.

This technique exploits the intensity-dependent variation in the refractive index and absorption exhibited by a sample when it interacts with a focused Gaussian laser beam. A laser source is directed and focused using a plano convex-lens, generating a spatial intensity distribution characterized by the beam waist (ωo) and Rayleigh length (Z_R). The sample stage is translated throughout the propagation (Z) axis within the focal region, and the transmitted light is recorded under two configurations.

Open aperture Z-scan

Within the open-aperture (OA) arrangement, the detector collects all transmitted light, making the setup sensitive to nonlinear absorption phenomena, including two-photon absorption or saturable absorption. The transmittance minimum (ΔTmin) is employed to evaluate the nonlinear absorption coefficient (β) as;

$$\beta = 2\sqrt{2}.\Delta T_{min}/I_o.L_{eff} \quad (4)$$

L_{eff} is the sample's effective optical path length (L_{eff}), calculated using the relation below.

$$L_{eff} = 1 - e^{-\alpha L} \quad (5)$$

Where Io represents the peak intensiy at the focal point of the beam, while Leff

corresponds to the effective optical path length of the sample.

Closed aperture Z-scan

In the closed aperture arrangement, a finite aperture is positioned before the detector, enabling measurement of nonlinear refraction. The peak to valley transmittance (ΔTp-v) corresponds to the on axis nonlinear phase shift ($\Delta\phi_o$)

$$\Delta\phi_o = \Delta Tp\text{-}v/0.406(1\text{-}S)^{0.25} \quad (6)$$

The nonlinear refractive index is subsequently determined through

$$n_2 = \Delta\phi_o.\lambda/2\pi.Leff.Io \quad (7)$$

Where λ represents laser wavelength and S denotes the linear transmittance of the aperture

The linear transmittance of the aperture was determined from the following equation:

$$S = 1 - \exp -2r_2^a/w^2 \quad (8)$$

The Z-scan method is widely regarded as a standard characterization approach for nonlinear optical crystal due to its precision, simplicity, and versatility.

The magnitude of the third-order nonlinear optical susceptibility ((3)) of the material was derived from the real and imaginary components. The real part of the susceptibility, associated with intensity-dependent refractive effects, was calculated as

$$X_{Real}^{(3)} = 10^{-4} (\epsilon o.c2.no.n2/\pi) \text{ (in esu)} \quad (9)$$

while the imaginary part, representing nonlinear absorption, was determined from

$$\chi_{img}^{(3)} = (10^{-2} \epsilon o.c2.\lambda.\beta/4\pi^2) \text{ (in esu)} \quad (10)$$

The overall magnitude of the third order susceptibility was obtained based on material's nonlinear optical response.

$$\chi (3) = \sqrt{(Re(3))2 + (Img\chi(3))2} \text{ (in esu)} \quad (11)$$

The Rayleigh length (ZR) of 1.29 mm of the NLO crystal was calculated from the experimental parameters. It was found that when (L < ZR), with the negative (-Z) to positive (Z) axis oriented within the laser propagation direction, the conditions was satisfied. The Rayleigh length (Z_R) of the NLO crystal was determined as 1.29 mm, ensure proper focusing and accurate measurements in the Z-scan analysis **[35]**.

A pronounced peak to valley feature in the open-aperture Z-scan indicates that the material absorption rises with increasing light intensity, corresponding to β > 0 and signifying reverse saturable absorption

Observation of the valley subsequent to a peak in the closed aperture Z-scan signifies intensity-dependent refraction, with $n_2 > 0$, signifying self–focusing in the sample.

In closed aperture arrangement, the nonlinear refractive index (n_2) was measured at 2.40 x

10^{-15} m^2/W. In the open aperture, the nonlinear absorption coefficient was calculated as 4.38 x 10^{-8} m/W for LASPOD material. The real value is calculated as 1.37 x 10^{-13} esu, and the Imaginary value is measured as 1.26 x 10^{-11} esu. The overall magnitude of the third order susceptibility at 1.26 x 10^{-11}esu for LASPOD crystals.

This calculated parameter reflects the overall efficiency of nonlinear interactions in the material, rendering it appropriate for NLO applications, including supercontinuum generation, ultra fast optical switching, optical data processing, and photonic device fabrication. Fig 9 (a) and fig 9 (b) depict the open aperture and closed aperture Z-scan profiles of the material respectively. Table 8 lists the Z-scan parameters employed to measuring the NLO properties of the sample.

In, open aperture the material exhibits (RSA) are widely used in Laser protection, photonic devices and sensor safety.

In closed aperture configuration, the self focusing behaviour is exhibited by LASPOD single crystals enables diverse applications including frequency conversion, ultrafast optical switching, optical limiting, optical data storage and processing.

The open aperture configuration Z-scan arrangement of the material exhibited a distinct valley to peak transmittance graph, indicative of reverse saturable absorption (RSA). The positive value of the nonlinear absorption coefficient (β) suggests that the sample demonstrates intensity-dependent enhancement of absorption, where higher incident light intensities lead to increased absorption. This nonlinear optical behavior indicates the presence of strong excited-state absorption, making the material suitable for applications that require controlled attenuation of high intensity light, such as optical limiting, laser protection, and photonic switching devices. The observed RSA behaviour suggests that the material could effectively protect sensitive optical components from laser-induced damage while enabling dynamic modulation of light, which is highly desirable in the design of advanced photonic systems.

The closed aperture Z-scan measurement for the sample displayed a small valley to peak subsequently succeeded by a larger valley in the transmittance profile, characteristic of self-focusing nonlinear refraction. This indicates a positive nonlinear refractive index (n_2), where the refractive index increases with light intensity, causing a spatial phase modulation of the transmitted Gaussian beam. The peak to valley transmittance differences (ΔT (p-v)) was used to calculate the on axis nonlinear phase shift ($\Delta\phi_o$), confirming a significant third order nonlinear response. Such positive self focusing behaviour is promising for all optical switching, optical phase modulation, and photonic signal processing, enabling efficient light control without substantial energy loss **[36].**

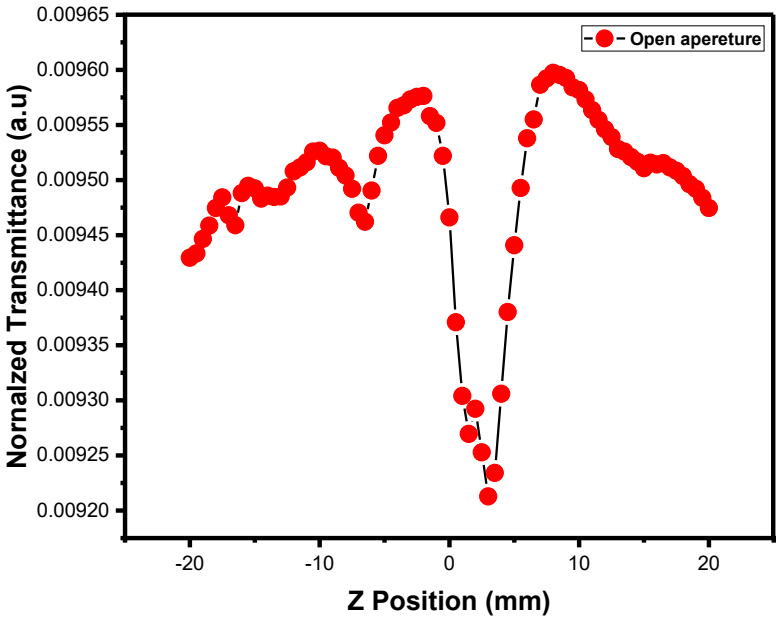

Fig 9 (b). Open aperture Z-scan

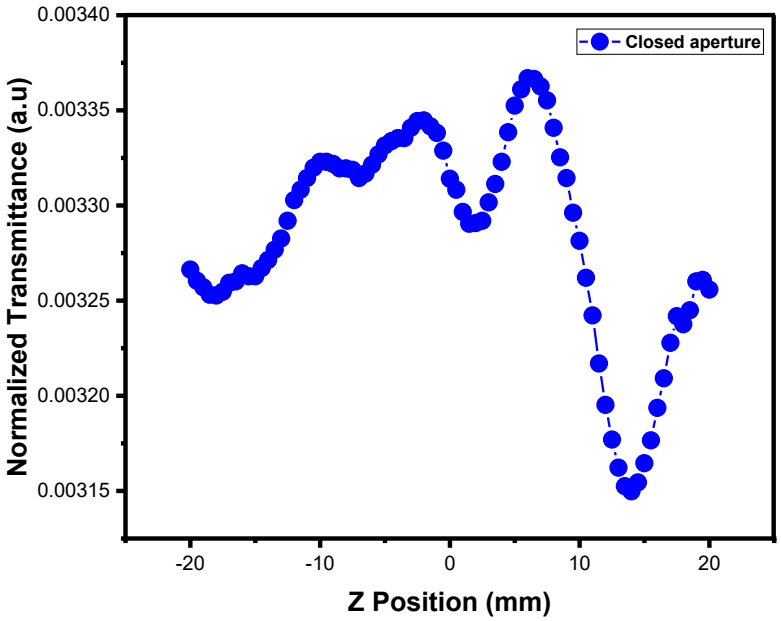

Fig 9 (c). Closed aperture Z-scan

Table 8.

Z-scan measurements showing the experimental parameters and corresponding values.

Parameter	Value
Sweeping Distance	40.0 mm
Step Distance	0.5 mm
Bandwidth	High
Wavelength (λ)	632.8 nm
Power of the Laser (E_P)	12.0 mW
Diameter of the Laser beam (d)	5 mm
Focal Length of the Lens (f)	200 mm
Radius of the Aperture (r_a)	2 mm
Radius of the beam at Aperture (w_a)	4.5 mm
Z-Scan Sample Thickness (L)	1 mm
Linear refractive index (n_o)	1.5
Transmittance (T)	70 %

9). Photoluminescence studies

Photoluminescence (PL) studies is a non-destructive optical technique employed to investigate the electronic and optical behavior of crystal. When a material is excited by light, it release during the radiative recombination of electrons return to lower energy states. The emissions spectrum reveals information about band gap, defects and crystalline quality. PL is widely applied in characterizing NLO materials for photonics and optoelectronic

devices **[37]**. The first peak observed around (466 nm), The second peak observed at (536 nm), and thus the third peak, appearing at (822 nm). The band gap (E_g) of a materials can be evaluated using photoluminescence analysis. In PL, the main emission peak usually corresponds to the recombination between electrons and holes from the conduction band to the valence band **[38]**.

By converting this emission wavelength (λ) into energy from the formula E (g) = 1240 /λ (nm), you can estimate the bandgap.

The crystal shows a PL emission maximum peak at (466 nm), the band gap of 2.662 eV. The photoluminescence emission at 2.662 eV (466 nm) indicates strong optical activity, rendering the material appropriate for nonlinear optical applications including Frequency doubling, optical switching, and electro-optic modulation **[39]**. Fig 10 depicts the photoluminescence (PL) graph of the sample, illustrating its emission characteristics under excitation.

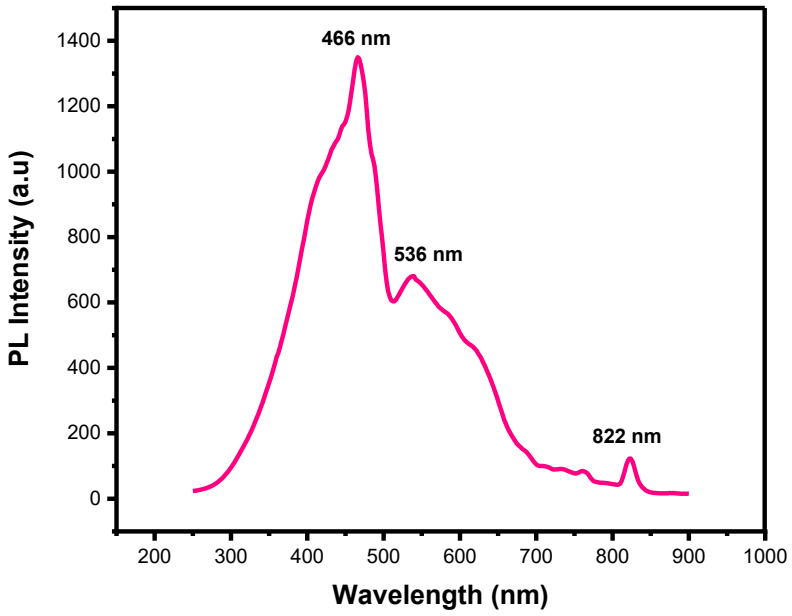

Fig 10. PL graph showing wavelength versus emission intensity

10). 1H and 13C FT NMR

FT-NMR spectroscopy serves as an effective tool for identifying the molecular structure in grown crystals. The technique is especially useful to verify the purity and structural integrity of organic nonlinear optical crystals **[40]**. The structural properties of the compound was carried out through FT-NMR spectroscopy to verify the molecular arrangement and chemical environmental of the protons. The molecular framework of the

prepared material was conducted to verify through 1H and 13C fourier transform NMR (FT-NMR) spectroscopy. The 1H NMR spectrum displayed three distinct downfiled signals at δ 4.118, 4.105, and 4.091 ppm, which can be attributed to protons attached to electronegative atoms or located in a deshielded chemical environment. Additionally, multiplets signals appearing at δ 2.814, 2.811, 2.799, and 2.798 ppm correspond to protons in more shielded aliphatic environments, indicating the presence of methylene or methane groups within the molecule **[41]**.

The 13C NMR spectrum exhibited resonances at δ 273.33, 171.21, and 164.03 ppm, consistent with carbonyl carbons in conjugated or highly deshielded positions, while signals at δ 49.46 and 33.65 ppm correspond to aliphatic carbons, further supporting the presence of methylene and quaternary carbon centers. Overall, the observed NMR chemical shifts corroborate the predicted molecular configuration and verify the successful synthesis of the target compound **[42]**. Fig 9 (a to c) show the 1H FT-NMR spectra, while Fig 9 (d) presents the 13C FT-NMR corresponding to the sample.

1H FT-NMR

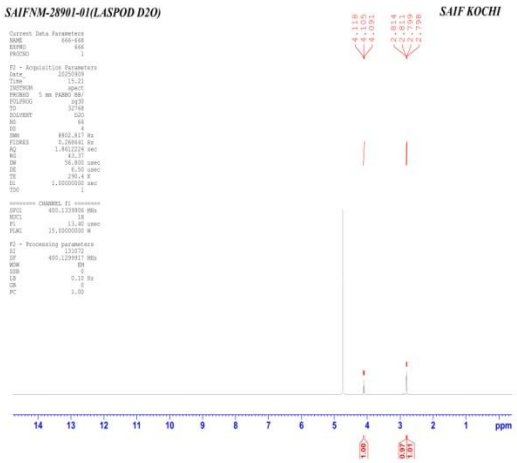

Fig 11 (a) 1H FT-NMR spectra of the sample showing proton chemical shift

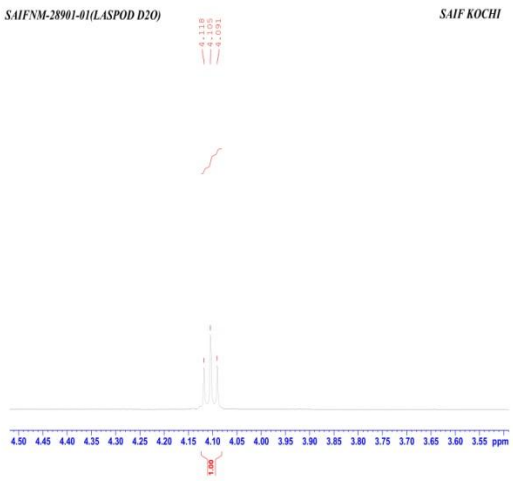

Fig 11 (b) 1H FT-NMR spectra of the material showing proton chemical shift

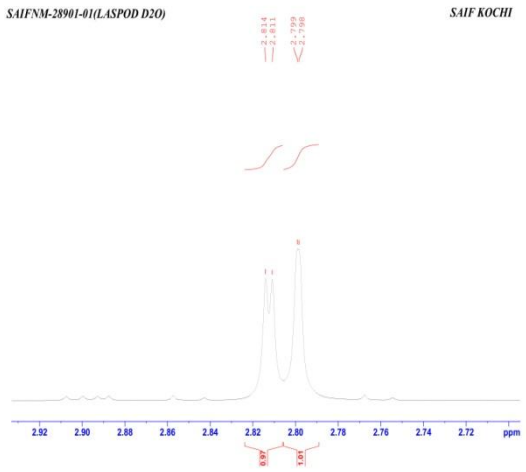

Fig 11 (c) 1H FT-NMR spectra of the material showing proton chemical shift

13C FT-NMR

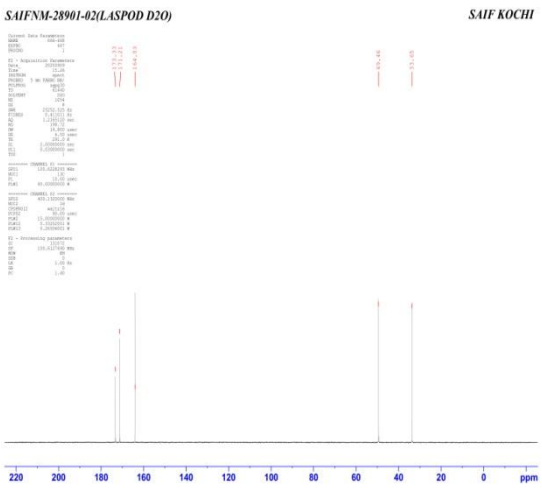

Fig 11 (d). 13 C FT NMR spectra of the material showing carbon chemical shifts

11). Vickers Microhardness test

The correlation of microhardness (Hv) on the indentation diagonal length (d) in (μm) was analyzed to evaluate the structural integrity and defect distribution of the synthesized material.

The relation between the indentation diagonal d (μm) and the corresponding Vickers Hardness number (Hv), expressed in (kg/mm^2), was systematically examined to assess the mechanical characteristics of the prepared material **[43]**. The observed relationship between Hv on D provides significant insights into the resistance of the material against localized plastic deformation, as well as the role of intrinsic defects, dislocation defects and lattice imperfections in governing the overall mechanical stability of the crystal lattice **[44]**.

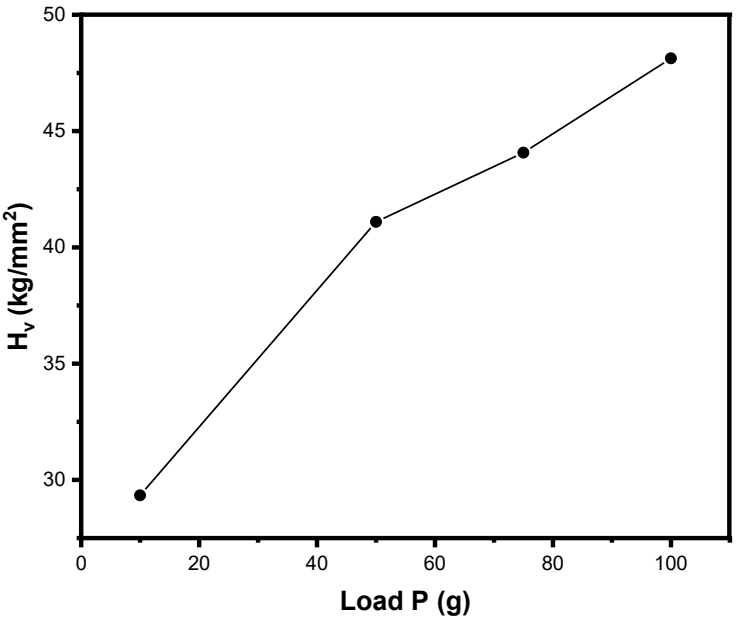

Fig 12 (a). Vickers hardness Hv (kg/mm^2) variation with applied load P (g)

Microhardness measurements of the sample were conducted under applied loads of 10, 50, 75 and 100g to study the mechanical response and investigate the load-dependent indentation size effect (ISE). The results demonstrated a clear increase in vickers hardness (Hv) with increasing load, confirming the presence of ISE, where lower loads produced comparatively lower hardness values and higher loads resulted in enhanced H_v. This load-dependent variation in hardness reflects the influence of geometrically necessary dislocations and microstructural constraints on the material's resistance to deformation **[45]**. The observed trend offered detailed understanding of the intrinsic mechanical characteristics of the crystal and emphasizes the significance of ISE in interpreting the hardness behavior under varying applied stresses **[46]**. Fig 12 (a) illustrates the dependence of vickers hardness (Hv in kg/mm^2) on the applied load P (g)

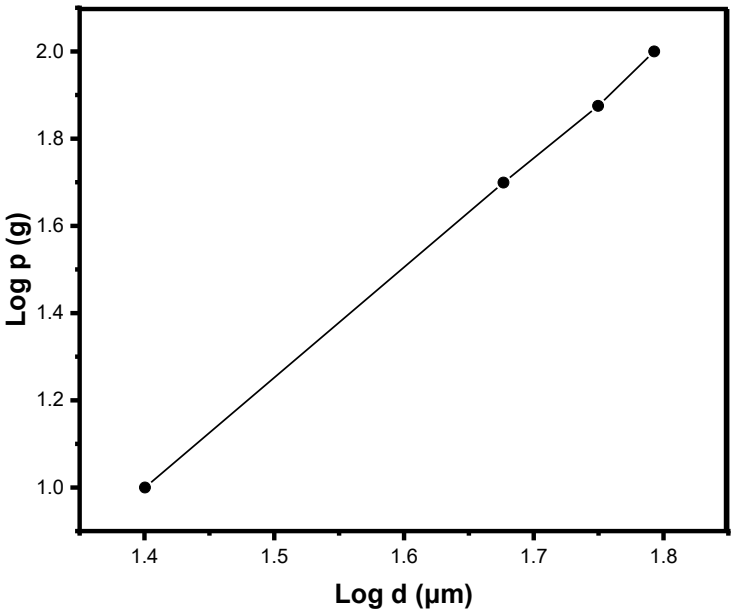

Fig 12 (b).Log-Log plot of identional diagonal d (µm) versus applied load P (g)

A graph of log d (µm) versus Log P (g) was constructed , where Log d values of 1.400, 1.677, 1.750, and 1.793 corresponded to applied loads P of 1, 1.699, 1.875, and 2 respectively. The slope of the linear fit yielded a work-hardening exponent (n) of 2.53, indicating that the sample behaves as a relatively hard material **[47]**. The observed trend indicates a reverse indentation size effect (RISE), where hardness increases with increasing load, reflecting the crystal's strong resistance to deformation and the influence of microstructural constraints on its mechanical response. These results offer detailed understanding of the intrinsic hardness characteristics and load-dependent deformation behavior of the material **[48]**. Fig 12 (b) illustrates the plot of log indentation diagonal log d (µm) versus applied load log P (g).

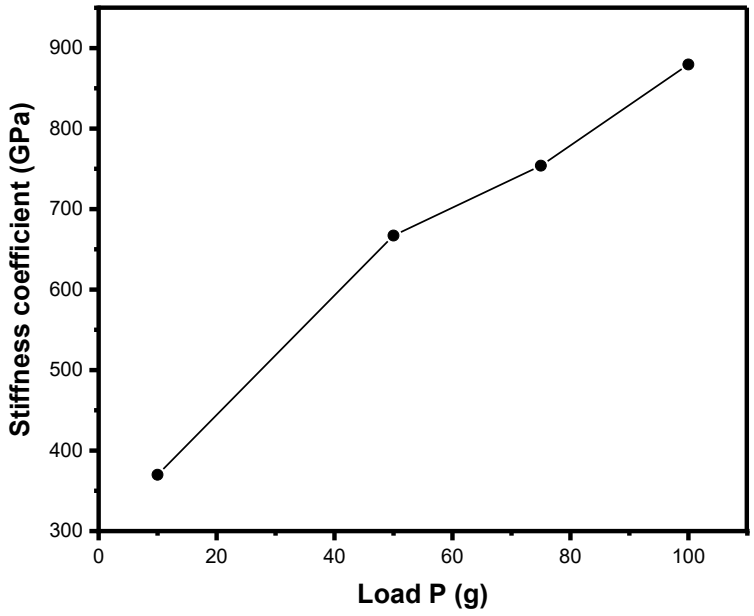

Fig 12 (c). Dependence of stiffness coefficient (GPa) on applied Load P (g)

Stiffness measurements of the sample were performed under varying applied loads, and the results revealed a progressive increase in the stiffness coefficient (C11) with increasing load **[49]**. This trend reveals that the sample exhibits enhanced resistance towards deformation under applied higher loads, reflecting to deformation under higher loads, reflecting its intrinsic mechanical strength and load- dependent behaviour. A corresponding graph of Log C_{11} versus Log P further illustrates the systematic variation of stiffness, providing insights into the mechanical characteristics of the crystal **[50]**. Fig 12 (c) depicts the dependence of the stiffness coefficient (GPa) on the applied load P (g).

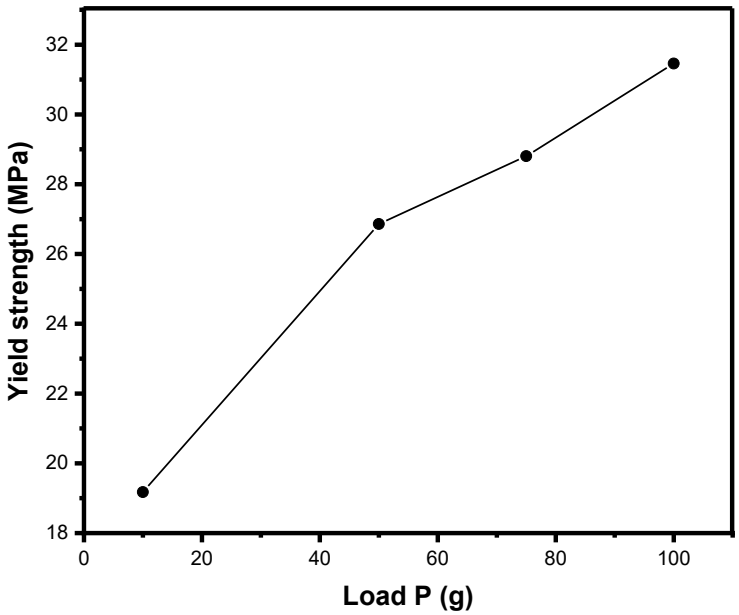

Fig 12 (d). Dependence of yield strength (MPa) on applied load P (g)

Yield strength measurements of the sample were carried out under varying applied loads, and the results exhibited a progressive increase in yield strength with increasing load **[51]**. This load dependent behaviour reflects the material's enhanced resistance to plastic deformation under higher stresses and provides insight into its intrinsic mechanical stability and deformation characteristics **[52]**. Fig 12 (d) depicts the dependence of yield strength (MPa) on the applied load P (g).

12). Antibacterial activity

The Antibacterial efficiency of the prepared NLO material was examined towards both Gram-Positive and Gram-negative bacterial strains **[53]**. The investigation was conducted to evaluate the ability of the material to suppress microbial growth, thereby highlighting its potential role in biomedical applications **[54]**. The results indicated a significant inhibitory effect, suggesting that the optical material not only possesses desirable nonlinear optical properties but also exhibits promising antibacterial activity, making it a multifunctional candidate for future research in Biomedical and pharmaceutical fields **[55, 56]**.

The antibacterial efficiency of the sample was investigated towards Gram-positive (S. aureus) and Gram-negative (E. coli) bacteria through the agar well diffusion technique **[57]**. The analysis indicated that the material exhibited clear inhibition zones for each bacterial strains, indicating effective antibacterial action. Notably, the inhibition was observed towards both gram-positive and gram-negative bacteria, suggesting that the sample possesses broad-spectrum antibacterial potential **[58]**.

The comparision with the control further confirmed the efficacy of the sample, and the observed variation in susceptibility among the bacterial types can be ascribed to structural differences in the bacterial cell wall, which influence the interaction of the antibacterial agents with the bacterial membrane **[59]**. These findings highlight the potential of the sample as an effective antimicrobial material for further biological applications **[60]**. Figure 13 (a) and figure 13 (b) show the antibacterial efficiency of the sample towards S. aureus and E. coli, respectively. Table 9 presents the antibacterial efficiency of the sample towards various bacterial strains, showing the measured zones of inhibition in comparision with the control plates.

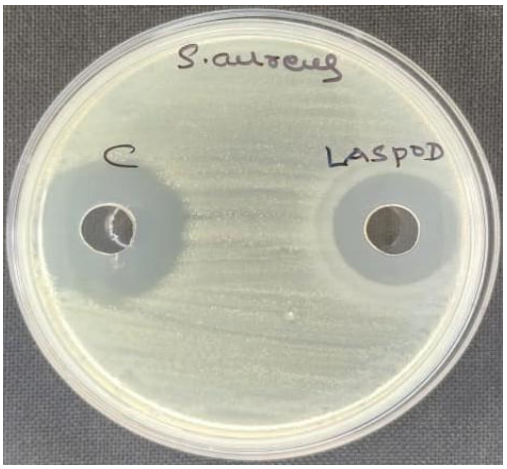

Fig 13 (a). Antibacterial Activity – S .aureus

Fig 13 (b) Antibacterial activity – E. coli

Table. 9

The zone of inhibition and control plate observations for various bacterial strains

S. NO	Strain	Gram reaction	Control	Zone of inhibition (mm)
1	S. aureus	+Gram	25	20
2	E. coli	- Gram	25	21

Conclusion

In, powder analysis revealed the lattice parameters a = 6.34 A° , b = 7.27 A°, c = 10.56 A° and angle are α = 93.89 ° , β = 100.19 ° , γ = 98.14 °, V = 4, and also confirmed the Triclinic crystal structure of the LASPOD material. The powder analysis revealed a strain value of 3.86 x10^{-5} indicating the presence of lattice distortions and internal stress within the fabricated crystal. The fourier transform infrared spectroscopy confirmed the

identification of characteristic functional moieties, there by verifying the molecular composition and structural integrity of the material. In UV-DRS studies of the grown crystal revealed its absorbance, Transmittance (%) behaviour, from which crucial optical properties they are optical conductivity, Refractive index and Reflectance were determined. CHN analysis is an elemental analysis technique for quantifying the elemental composition of carbon (31.78 %), Hydrogen (5.64 %) and Nitrogen (12.01 %) in a compound. EDX studies demonstrated the atomic consituents in the synthesized crystal, indicating the detection of all expected elements without detectable impurities, thereby supporting the material's compositional purity and structural stability. Thermal analysis of the grown single crystal through TG-DTA along with kinetic evaluations via kissinger's methods, provided detailed insights into its activation energy, decomposition pattern and thermal stability. The maximum peak observed at (466 nm) corresponding to the bandgap energy of 2.662 eV. 1H and 13C FT-NMR spectroscopy of the crystal confirmed its molecular framework and chemical environmental of constituent atoms, providing detailed insights into functional moieties and intramolecular interactions within the crystal lattice. In Z-scan analysis the nonlinear absorption coefficient is 4.38 x 10^{-8} m/W, the nonlinear refractive index is 2.40 x 10^{-15} m^2/W and then third order susceptibility of the LASPOD crystals is 1.26 x 10^{-11} esu. Microhardness analysis showed the relationships between indentation size and hardness reflecting the mechanical properties of the synthesized material. The antibacterial activity test revealed a zone of inhibition of 20 mm towards S. aureus and 21 mm against E. coli, confirming the antibacterial effectiveness of the sample.

References

[1]. N. Rajasekar, K. Balasubramanian. Crystallization and multifaceted characterization of L-Asparagine monohydrate single crystals for structural, spectroscopic, Optical, Thermal and morphological analysis toward for Third order NLO applications. International Journal of Applied Mathematics. Volume 38, No. 10s, (2025). ISSN: 1311-1728 (printed version); ISSN: 1314-8060 (on-line version)

DOI : https://doi.org/10.12732/ijam.v38i10s.992

[2]. N. Rajasekar, K. Balasubramanian. Advanced growth and multifunctional characterization of L-Threonine single crystals: comprehensive Insights for structural, Functional, optical, Mechanical, Antibacterial and Thermal properties with potential in optoelectronics, Photonics and nonlinear optical applications. The bioscan an international quarterly journal of life science (www.thebioscan.com). 21(1): 685-731, (2026). ISSN: 0973-7049 (P).

DOI: 10.63001/tbs.2026.v21.i01.pp685-731

[3]. P. Praveen kumar, V. Manivannan, P. Sagayaraj, and J. Madhavan. Growth and

characterization of pure and doped NLO L-arginine acetate single crystals. Bull. Mater. Sci., Vol. 32, No. 4, August 2009, pp. 431–435.

[4]. D. Kalaiselvi, R. Mohan Kumar, and R. Jayavel. Single crystal growth and properties of semiorganic nonlinear optical L-arginine hydrochloride monohydrate crystals. Cryst. Res. Technol. 43, No. 8, 851 – 856 (2008).

DOI : 10.1002/crat.200711133

[5]. Sonia, N. Vijayan, Mahak Vij, Kanika Thukral, Naghma Khan, D. Haranath, Rajnikant, M.S. Jayalakshmy , Investigation on the key aspects of L-arginine Para nitrobenzoate monohydrate single crystal: A non-linear optical material. Cjche. (2018).

DOI : 10.1016/j.cjche.2018.06.029

[6]. K. Vasantha, S. Dhanuskodi. Single crystal growth and characterization of phase-matchable l-arginine maleate: a potential nonlinear optical material. Journal of Crystal Growth 269 (2004) 333–341.

DOI : 10.1016/j.jcrysgro.2004.04.113

[7]. P. Vasudevan , S. Gokul Raj , S. Sankar. Synthesis and characterization of nonlinear optical L-arginine semi-oxalate single crystal. Spectrochimica Acta Part A: Molecular and Biomolecular Spectroscopy 106 (2013) 210–215.

DOI : http://dx.doi.org/10.1016/j.saa.2012.12.098

[8] G. Shanmugam, S. Brahadeeswaran. Spectroscopic thermal and mechanical studies on 4-methylalanilium P-Tolunenesulfonate-A new organic NLO single crystal. Spectrochimica Acta Part A: Molecular and Biomolecular Spectroscopy. 95, (2012), 177-183.

http://dx.doi.org/10.1016/j.saa.2012.04.100

[9]. D. Kalaiselvi, R. Mohan Kumar, R. Jayavel . Growth and characterization of nonlinear optical L-arginine maleate dihydrate single crystals. Materials Letters 62 (2008) 755–758.

DOI : 10.1016/j.matlet.2007.06.054

[10]. A. Hemalatha, S. Arulmani, P. Sanjay , K. Deepa , J. Madhavan and S. Senthil. Growth and Characterization of L-Leucenium Hydrogen Maleate Single Crystals for Nonlinear Optical Applications. IOP Conf. Series: Materials Science and Engineering. 360, (2018), 012044.

DOI : 10.1088/1757-899X/360/1/0120

[11]. K. Naseema, Sarath Ravi, Rakhi Sreedharan. Studies on a novel organic NLO single crystal : L-asparaginium oxalate. Chinese Journal of Physics. 60, (2019), 612-622.

DOI : https://doi.org/10.1016/j.cjph.2019.05.037

[12]. M. Porchelvi and R. Rajasekaran. Synthesis, Growth and characterization of L-Histidine doped Potassium dihydrogen

Phosphate(LHKDP) crystals. OSR Journal of Applied Chemistry (IOSR-JAC) (www.iosrjournals.org). Volume 12, Issue 1 Ser. I (January. 2019), PP 25-33. e-ISSN: 2278-5736

[13]. D. Kalaiselvi, R. Mohan Kumar, and R. Jayavel. Growth, optical and thermal studies of nonlinear optical L-arginine perchlorate single crystals. Cryst. Res. Technol. 43, No. 6, 645 – 650, (2008).

DOI : 10.1002/crat.200711067

[14]. R. Sankar, R. Muralidharan, C.M. Raghavan, R. Jayavel . Structural, thermal, mechanical and optical properties of l-arginine diiodate crystal: A new nonlinear optical material. Materials Chemistry and Physics. 107, (2008), 51–56.

DOI : 10.1016/j.matchemphys.2007.06.039

[15]. M. Prakash , M. Lydia Caroline , D. Geetha. Growth, structural, spectral, optical, and thermal studies on amino acid based new NLO single crystal: L-phenylalanine-4-nitrophenol. Spectrochimica Acta Part A: Molecular and Biomolecular Spectroscopy. 108, (2013), 32–37.

DOI : http://dx.doi.org/10.1016/j.saa.2013.01.078

[16]. S. Dhanuskodi , P.A. Angeli Mary, K. Vasantha. Spectroscopic and optical studies on pure and doped single crystals of sulphate-mixed L-arginine phosphate monohydrate*/a nonlinear optical crystal. Spectrochimica Acta Part A. 59, (2003), 927-935.

[17]. A. Senthamizhan , K. Sambathkumar , S. Nithiyanantham. Physico-chemical, structural, optical and NLO studies on pure and La3+ doped L-arginine acetate crystals. Materials Science for Energy Technologies. 3, (2020), 282–288.

DOI : https://doi.org/10.1016/j.mset.2019.11.005

[18]. R. Muralidharan, R. Mohankumar, R. Jayavel, P. Ramasamy. Growth and characterization of L-arginine acetate single crystals: a new NLO material. Journal of Crystal Growth. 259, (2003), 321–325.

DOI : 10.1016/j.jcrysgro.2003.07.021

[19]. Pratik M. Wankhade, Al.B. Gambhire, G.G. Muley, Influence of urea doping on optical, thermal, mechanical and electrical properties of L-arginine phosphate monohydrate crystals for NLO applications, Optik - International Journal for Light and Electron Optics. (2015).

DOI : http://dx.doi.org/10.1016/j.ijleo.2015.12.091

[20]. K. Parasuraman, K. Sakthi Murugesan, R. Samuel Selvaraj , S. Jerome Das , R. Uthrakumar , B. Milton Boaz. Unidirectional growth, optical, mechanical and dielectric studies on a novel NLO crystal: l-Arginine 4-nitrophenolate 4-nitrophenol dihydrate. Optik, (2014).

DOI : http://dx.doi.org/10.1016/j.ijleo.2014.01.056

[21]. P. Vasudevan, S. Sankar, and D. Jayaraman. Synthesis, Optical and Electrical Studies of Nonlinear Optical Crystal: L-Arginine Semi-oxalate. 128 Bull. Korean Chem. Soc. (2013), Vol. 34, No. 1.

DOI : http://dx.doi.org/10.5012/bkcs.2013.34.1.128

[22]. S. Janarthanan, T. Kishore kumar, S. Pandi, and D. Prem anand. Growth and spectroscopic studies of L-Arginium formate NLO single crystals. Indian journal of pure and applied physics. Vol. 47, may. 2009, pp-332-336.

[23]. S. Aruna, A. Anuradha, Prema C Thomas, M. Gulam Mohamed, S. A. Rajasekar, M. Vimalan, G. Mani, and P. Sagayaraj. Growth, Optical, and thermal studies of L- Arginine perchlorate- A Promising nonlinear optic single crystals. Indian journal of pure and applied physics. Vol. 45, june 2007, pp: 524-528.

[24]. S. Sathiskumar, T. Balakrishnan, K. Ramamurthi, S. Thamothran. Synthesis, Structure, crystal growth and characterization of a novel semiorganic nonlinear optical L-proline lithium bromide monohydrate single crystal. Spctrochimica Acta Part A: molecular and Biomolecular spectroscopy. 138 (2015) 187-194.

DOI : http://dx.doi.org/10.1016/j.saa.2014.11.004

[25]. T. Prasanyaa and M. Haris. Growth and characterization of semiorganic NLO L-arginine trifluoroacetate (LATF) added KDP single crystals. Archives of Physics Research, 2011, 2 (4) : 60-66.

[26]. M. Saravanan, A. Senthil, S. Abraham Rajasekar. Crystal growth, solubility, structural, optical, thermal, mechanical and electrical studies of l-arginium adipate: An organic nonlinear optical material. Optik (2015).

DOI : http://dx.doi.org/10.1016/j.ijleo.2015.10.223

[27]. A.S. Haja Hameed , P. Anandan , R. Jayavel , P. Ramasamy , G. Ravi. Synthesis, growth and characterization of nonlinear optical material: l-arginine fluoride. Journal of Crystal Growth. 249, (2003), 316–320.

DOI : https://doi.org/10.1016/S0022-0248(02)01978-4

[28]. P. V. Radhika , K. Jayakumari , C. K. Mahadevan. Formation and properties of L-arginine acetate single crystals doped with hydrochloric acid. IOSR Journal of Applied Physics (IOSR-JAP) (www.iosrjournals.org) .Volume 6, Issue 4 Ver. III (Jul-Aug. 2014), PP: 19-29. e-ISSN: 2278-4861

[29]. K. Meera, R. Muralidharan, R. Dhanasekaran , Prapun Manyum , P. Ramasamy. Growth of nonlinear optical material: L-arginine hydrochloride and its characterisation. Journal of Crystal Growth, 263, (2004), 510–516.

DOI : 10.1016/j.jcrysgro.2003.11.093

[30]. D. Sankar, Vinay Raj Menon, P. Sagayaraj, J. Madhavan. Thermal, mechanical, electrical, linear and nonlinear optical properties of L-arginine dihydrofluoride single crystal. Physica B. 405, (2010), 192–197.

DOI : 10.1016/j.physb.2009.08.061

[31]. A. Pricilla Jeyakumari, S. Dhanuskodi, S. Manivannan. Phase matchable semiorganic NLO material for frequency doubling: l-Arginine tetrafluoroborate. Spectrochimica Acta Part A. 63, (2006), 91–95.

DOI : 10.1016/j.saa.2005.04.051

[32]. A. Senthil , T. Bharanidharan , M. Vennila , Elangovan K d , S. Muthu. Crystal growth, Hirshfeld analysis, optical, thermal, mechanical, and third-order non-linear optical properties of Cyclohexylammonium picrate (CHAP) single crystal. Heliyon. 10, (2024), e28002.

[33]. P. Umarani, S. Kalainathan, and K. Jagannathan. Third Order Nonlinear Properties of Pure and Na Doped L-Arginine Acetate Single Crystal by Z-scan Technique. Oriental journal of chemistry. ISSN: 0970-020 X (2016), Vol. 32, No. (1): Pg. 213-218

DOI : http://dx.doi.org/10.13005/ojc/320122

[34]. P. Sangeetha, M. Nageshwari, C. Rathika Thaya Kumari, S. Sudha, P. Jayaprakash, M. Lydia Caroline, G. Mathubala, G. Vinitha, A. Manikandan. Linear and nonlinear optical investigation of L-arginium adipate single crystal for photonic applications. Journal of Materials Science: Materials in Electronics. (2020).

DOI : https://doi.org/10.1007/s10854-020-04015-0

[35]. V. Natarajan , T. Sivanesan and S. Pandi. Third order non-linear optical properties of L-arginine hydrochloride monohydrate single crystals by Z-Scan technique. Indian Journal of Science and Technology. Vol. 3, No. 8, (Aug 2010).

[36]. I. Epsy Devakirubai , S.M. Ravi Kumar, S.E. Allen Moses, R. Gunaseelan. Probing optical (2nd and 3rd order), mechanical and thermal traits of L-arginine hydrochloride monohydrate (LAHCM) NLO crystal for optoelectronics device applications. Materials Today: Proceedings.

DOI : https://doi.org/10.1016/j.matpr.2020.08.696

[37]. S. Sakthy Priya , A. Alexandar , P. Surendran , A. Lakshmanan , P. Rameshkumar , P. Sagayaraj. Investigations on nucleation, HRXRD, optical, piezoelectric, polarizability and Z-scan analysis of Learginine maleate dihydrate single crystals. Optical Materials. 66, (2017), 434 – 441.

DOI : http://dx.doi.org/10.1016/j.optmat.2017.02.041

[38]. A. Anandhan, C. Sivasankari, M. Saravanabhavan, V. Siva, K. Senthil, Synthesis, crystal structure, spectroscopic investigations, physicochemical properties of

third-order NLO single crystal for optical applications, Journal of Molecular Structure (2019),

DOI : https://doi.org/10.1016/ j.molstruc.2019.127400

[39]. Paul M. Dinakaran, S. Kalainathan. Synthesis, growth, structural, spectral, linear and nonlinear optical and mechanical studies of a novel organic NLO single crystal 4-Bromo 4-Nitrostilbene (BONS) for nonlinear optical applications. Optical Materials. (2012).

DOI : http://dx.doi.org/10.1016/j.optmat.2012.11.007

[40]. F. Ben Brahim, A. Bulou. Growth and spectroscopy studies of ADP single crystals with l-proline and l-arginine amino acids. Materials Chemistry and Physics. 130, (2011), 24–32.

DOI : 10.1016/j.matchemphys.2011.02.070

[41]. M. Lydia Caroline , M. Prakash , D. Geetha , S. Vasudevan. Growth, structural, vibrational, optical, laser and dielectric aspects of l-alanine alaninium nitrate single crystal. Spectrochimica Acta Part A. 79, (2011), 1936–1940.

DOI : 10.1016/j.saa.2011.05.094

[42]. Ramesh Rajendran, Thangammal Harris freeda, Udaya lakshmi kalasekar, Rajesh Narayanan peruma. Synthesis, Crystal growth and characterization of Organic NLO material: M-Nitroacetanilide. Advances in materials physics and chemistry. (2011), 1, 39-43.

DOI : 10.4236/ampc.2011.12007

[43]. S. Arjunana, A. Bhaskaran, R. Mohan Kumar, R. Mohanc, R. Jayavel. Effect of rare-earth dopants on the growth and structural, optical, electrical and mechanical properties of l-arginine phosphate single crystals. Journal of Alloys and Compounds. 506, (2010), 784–787.

DOI : 10.1016/j.jallcom.2010.07.070

[44]. D. Rajan Babu , D. Jayaraman , R. Mohan Kumar , G. Ravi , R. Jayavel. Growth aspects of semi-organic nonlinear optical l-arginine tetrafluoroborate single crystals. Journal of Crystal Growth. 250, (2003), 157–161.

DOI : 10.1016/S0022-0248(02)02254-6

[45]. G. Peramaiyan, P. Pandi , G. Bhagavannarayana , R. Mohan Kumar. Studies on growth, structural, dielectric, laser damage threshold, linear and nonlinear optical properties of methylene blue admixtured L-arginine phosphate single crystal. Spectrochimica Acta Part A: Molecular and Biomolecular Spectroscopy. 99, (2012), 27–32.

DOI : http://dx.doi.org/10.1016/j.saa.2012.08.087

[46]. T. Prasanyaa , M. Haris , V. Mathivanan , M. Senthilkumar , T. Mahalingam , V. Jayaramakrishnan. Synthesis and characterization of pure, urea and thiourea

doped organic NLO L-arginine trifluoroacetate single crystals. Materials Chemistry and Physics.

DOI : http://dx.doi.org/10.1016/j.matchemphys.2014.05.011

[47]. G. Parvathy , R. Kaliammal , K. Velsankar , M. Krishna Kumar , K. Sankaranarayanan , S. Sudhahar. Studies on structural, optical, homo-lumo and mechanical properties of piperazinium p-hydroxybenzoate monohydrate single crystal for nonlinear optical applications. Chemical Physics Letters. 758, (2020), 137934.

DOI : https://doi.org/10.1016/j.cplett.2020.137934

[48]. Anbuchezhiyan, S. Ponnusamy, C. Muthamizhchelvan, C. C. Kanakam, S. P. Singh, P. K. Pal, and P. K. Datta. Etching, microhardness and laser damage threshold studies of a nonlinear optical material: L-valine. The European physics journal applied physics. Eur. Phys. J. Appl. Phys. (2012), 58 : 10201

DOI : 10.1051/epjap/2012110358

[49]. Binitha. S. D, V. T. Jisha. Preparation and Antibacterial characterization of mixed crystals of tutton's salt $(NH_4)KZn(SO_4)2.6H_2O$. Journal of advanced scientific research. (2021), 12 (2), suppl 1 : 111-116. (ISSN 0976-9595).

[50]. P. Purushothaman, K. Arulaabaranam, P. Palani, N. Durairaj, and G. Mani. An organic (4-nitrophenyl) methionine single crystal:growth, optical properties and quantum chemical investigations for NLO device fabrication. Indian journal of physics. Volume. 97, pp. 3835-3851, (2023).

DOI : https://doi.org/10.1007/s12648-023-02711-1

[51].M. Ambrose Rajkumar, P. Ajit, S. anbarasu, Prem Anand Devarajan. Dielectric, Microhardness and Thermal properties of swift Ion (AU^{3+}) Irradiated NLO single crystal: 2-Amino-5-Nitropyridinium sulfamate (2A5NPS). Material science and Engineering. 1124, (2021), 012005

DOI : 1088/1757-899X/1124/1/012005

[52]. P. Sivakumar, V. Nadaraj. Growth, electrical, thermal, mechanical, and etching studies on 4-chloroanilinium hydrogen (2R, 3R)-tartrate monohydrate-an organic NLO single crystal. Material science-poland, 37 (3), 2019, pp. 310-316

[53]. P. Yasotha, R. Thiagarajan, P. Sagunthala. Growth, characterization, and antibacterial studies of L-Lysine single crystals added with a potassium bromide. Journal of applied physics (IOSR). Volume. 9, Issue. I, pp. 38-44. E-ISSN : 2278-4861.

DOI : 10.9790/4861-0901033844

[54]. M. Shanmuga sundaram, V. Vijayalakshmi, P. Dhanasekaran, O. N. Balasundaram, and S. Palaniswamy. Synthesis, Crystallization, Non Linear Optical, and Anti-bacterial Activity of L-Alanine sodium nitrate

single crystals. Journal of physics. Series. 1172, (2019), 012072.

DOI : 10.1088/1742-6596/1172/012072

[55]. P. Prabhukanthan, C. Raveendiran, G. Hariharan, Perumal seenuvasakumaran. Synthesis, crystal growth, crystal structure, optical, thermal, biological and NLO studies of hetrocyclic compound N-(1,3-benzothiazol-2-yl)-2-methoxybenzamide. Results in chemistry. 2, (2021), 100083.

DOI : https://doi.org/10.1016/j.rechem.2020.100083

[56]. C. Muthuselvi, S. Manisha, R. S. Prabhu. Growth, Spectral, Optical and Antibacterial Activity studies on Glycine Hydrofluoride Single Crystal. International Journal of Research in Engineering and science (IJRES) (www.ijres.org). Volume. 8, Issue. 11, (2020), pp. 45-53. (ISSN (online): 2320-9364), (ISSN (Print) : 2320-9356).

[57]. P. Lalitha , S. Arumugam , A. Sinthiya , C. Nivetha , M. Muthuselvam. Oxalic acid incorporated acetamide single crystal growth dynamics, characterization, NLO and antimicrobial activities via shock wave treatment. Results in Chemistry. 5, (2023), 100790.

DOI: https://doi.org/10.1016/j.rechem.2023.100790

[58]. K. Balakrishnan, S. Sakthy Priya, A. Lakshmanan, P. Surendran, Karthik Kannan, P. Geetha, G. Vinitha, P. Praveen Kumar, P. Rameshkumar. Physics and chemistry of solid states. V. 24, No. 1 (2023), pp. 46-55.

DOI: 10.15330/pcss.24.1.46-55

[59].N. Rajasekar, K. Balasubaramanian. Exploring structural, spectroscopic, Optical, Morphological, Mechanical, Antibacterial and Thermal parameters of Glycine A.R single crystals for advanced opto electronics, Photonics, Laser components and Nonlinear optical applications. Journal of nanotechnology perceptions (www.nano-ntp.com). 20 No. S 14 (2024), 4857-4893.

ISSN 1660-6795.

DOI : https://doi.org/10.62441/nano-ntp.vi.5784

[60]. N. Rajasekar, K. Balasubramanian. Design and evaluation of structural, spectroscopic, optical, thermal, morphological, and mechanical properties of L-alanine admixtured with oxalic acid dihydrate(1:1 ratio) single crystals for advanced optoelectronic, photonic, laser, and nonlinear optical applications. Journal of applied Bioanalysis. Vol. 11, No.6s, p. 1070-1093, December (2025). (ISSN 2405-710X)

DOI:http://doi.org/ 10.53555/jab.v11si6.2526